Research Article

iMedPub Journals
www.imedpub.com

Nano Research & Applications
ISSN 2471-9838

2018
Vol.4 No.2:4

DOI: 10.21767/2471-9838.100029

Widefield Confocal Microscope for Surface Wave K-Vector Measurement

Suejit Pechprasarn[1]*, Alexandr Melnikov[2], Terry WK Chow[2] and Michael G Somekh[3,4]

1 College of Biomedical Engineering, Rangsit University, Pathum Thani, Thailand
2 Department of Electronic and Information Engineering, Hong Kong Polytechnic University, Hong Kong SAR, P.R. China
3 Nanophotonics Research Centre, Shenzhen University, Shenzhen, P.R. China
4 Faculty of Engineering, University of Nottingham, Nottingham, UK

Corresponding author: Suejit Pechprasarn

suejit.p@rsu.ac.th

College of Biomedical Engineering, Rangsit University, Pathum Thani, 12000, Thailand.

Tel: +66-2997-2200-30

Citation: Pechprasarn S, Melnikov A, Chow TWK, Somekh MG (2018) Widefield Confocal Microscope for Surface Wave K-Vector Measurement. Nano Res Appl. Vol.4 No.2:4

Abstract

Optical surface waves are guided light on surface of optical structures. There are several optical structures that support optical surface waves, such as, nanostructures, gratings, optical waveguides and metamaterials. Optical surface waves have proven themselves very promising candidates for several applications including, biosensing, optical computing and optical circuitry. The characteristics of surface wave can be characterised by the wave vector (k-vector) of the surface wave. In this paper, we will discuss how a modified confocal microscope integrated with a phase spatial light modulator allows us to measure both the real part and the imaginary part (attenuation coefficient) of the surface wave k-vector. Surface plasmon resonance (SPR) excited on a uniform gold surface through Kretschmann configuration is employed as an example in this talk. Note that the system is not limited to the SPR. It is also applicable to other types of optical surface waves. We have demonstrated in our recent publication that the modified confocal not only provides the k-vector measurement both real and imaginary, it also allows us to separate different loss mechanisms in SPR. One limitation of the system was the single point detection. Here we will discuss the current stage of our development in widefield confocal surface plasmon microscope, which allows us to measure multiple points simultaneously. This has been achieved by integrating another amplitude spatial light modulator in the image plane of the objective lens. Use of orthogonal illumination patterns allows the image plane to be sequentially amplitude modulated and post-processed to recover the confocal image.

Keywords: Optical structures; Biosensing; Metamaterials; Light intensity

Received: August 07, 2018; **Accepted:** August 28, 2018; **Published:** August 31, 2018

Introduction

Recently scientists and engineers have been interested in applying optical surface waves [1] in several fields including biosensing [2-6], refractive index measurement [7-8], voltage sensing [9,10], ultrasonic detection [11-13], microscopy [5,14,15], optical computing [16] and optical circuitry [17] because of their unique optical properties. The optical surface waves are guided electromagnetic waves on surface of optical structures and devices, such as, metamaterials [18,19], gratings [20], nanostructures [21] and optical waveguides [22]. Optical surface waves can be characterised by their wave vector (k-vector) of the surface wave. The k-vector of optical surface wave consists of the real part k' and the imaginary part k''. The real part k' indicates the k-vector value, which the optical surface wave can be excited. The imaginary part k'' is the attenuation coefficient.

In this paper, surface plasmon resonance (SPR) excited on a uniform gold surface through Kretschmann configuration [23] is employed as an example of optical surface wave. Note that the methodology developed in this paper is not limited to only the SPR, but it is also applicable to other types of optical surface waves.

Since 2012, our group has been working on developing confocal surface plasmons microscopy [2,8,24-28] for quantitative interferometric imaging of biological samples. Simplified schematic for the confocal surface plasmon microscope for the SP wave vector measurement (k_{sp}) is shown in **Figure 1**. It depicts a defocused plasmonic gold sample 50 nm thick where the SPs are excited at its plasmonic angle ϑ_{sp}. The SPs excited at point 'a' depicted in **Figure 1** propagates to point 'b' and beyond it.

Confocal point pinhole allows reradiated SPs that appear to come from the focal point to be detected (path P2). The SPs reradiated from the other planes will be blocked by the confocal pinhole [24]. This allows us to have a well-defined detection path [2]. On the other hand, the light around the normal incident beam does not excite the SPs. This beam is directly reflected by the gold surface (path P1) and detected by the detector. These two beams can then form and interferometer. This modified confocal microscope is operated by defocusing the sample axis *z*, so called, *V(z)* measurement [28]. The other k-vector components that do not contribute the interferometric signal is then attenuated and blocked by amplitude pupil function as shown in **Figure 2**. The amplitude modulation is achieved by a phase spatial light modulator (phase-SLM) aligned so that it is in one of the conjugate planes of the back focal plane of the objective lens. The amplitude pupil function is modulated by an antiphase pair of consecutive pixels on the phase-SLM to cancel out the light intensity. The phase-SLM does not only provide the amplitude modulation, it also allows us to do electronic defocus by imposing the defocus phase profile on the phase-SLM as shown in **Figure 3(a)**. This enables us to the measure the *V(z)* curve without physical defocusing the sample [26] as shown in **Figure 3(b)**.

There are ripples in the *V(z)* curve shown in **Figure 3(b)**. These ripples can be related to the plasmonic angle ϑ_{sp} by the following equation:

$$\Delta z = \frac{\lambda}{2n(1-\cos\theta_{sp})} \quad (1)$$

Where Δz is the ripple period in the *V(z)* curve.

λ is the free space wavelength

n is the refractive index of the coupling media

θ_{sp} is the plasmonic angle

From the Equation (1), the recovered plasmonic angle is ~46.78° degrees, which agrees with the plasmonic angle of air backing sample. This also indicates the real part of the k_{sp} or k'_{sp}. perform phase stepping measurement [27]. the phase SLM can be employed to modulate the phase of either path P1 or P2 by 90 degrees step. This allows us to perform phase stepping measurement and recover the relative phase *φ(z)* of the SPs as shown in **Figure 4**. The *φ(z)* can be calculated by:

$$\phi(z) = \tan^{-1}\left(\frac{I_1 - I_3}{I_2 - I_4}\right) \quad (2)$$

Where *φ(z)* is the relative phase between the relative phase between the SP and the reference beam.

I_1, I_2, I_3 and I_4 are the *V(z)* curves in intensity with 0 degree, 90 degrees, 180 degrees and 270 degrees phase difference between path P1 and P2 respectively.

For the imaginary part of k_{sp} or k''_{sp}, this can be measured by blocking the P1 and allowing the path P2 to be detected by the confocal pinhole. The exponential decay curve can be detected by measuring the *V(z)* measurement. The attenuation coefficient can be determined by fitting a linear function to the natural logarithmic scale of the *V(z)* curve [8].

This system with a single phase SLM can only be used to scan a single object's point at a time. In this paper, we will demonstrate that by complementing the phase-SLM with another amplitude spatial light modulator (amp-SLM) this allows us to perform multipoint scanning simultaneously.

Materials and Methods

One of the main aims of this paper is to develop a widefield confocal surface plasmon microscope by designing a confocal microscope that allows us to measure multiple points simultaneously. Here it is achieved with sequential orthogonal coding in the image plane so different illumination points do not suffer from crosstalk. The uniqueness of the proposed system lies in the fact that a spatial light modulator (SLM) in the back focal plane can be used to use to perform additional processing to all the beams in parallel.

We have designed and constructed the microscope system based on two SLMs as shown in **Figure 5**. As indicated above the first SLM was aligned in one of the conjugate plane of the objective lens image plane serving as an amplitude SLM modulating the intensity profile of the objective lens image plane allowing the image plane to be spatially time-coded. The second SLM acts as a phase SLM providing phase modulation in the back focal plane (BFP). The experimental setup for the multiple point scanning

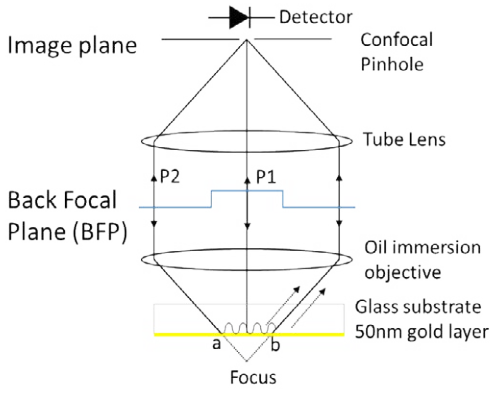

Figure 1 Simplified confocal surface plasmon microscope.

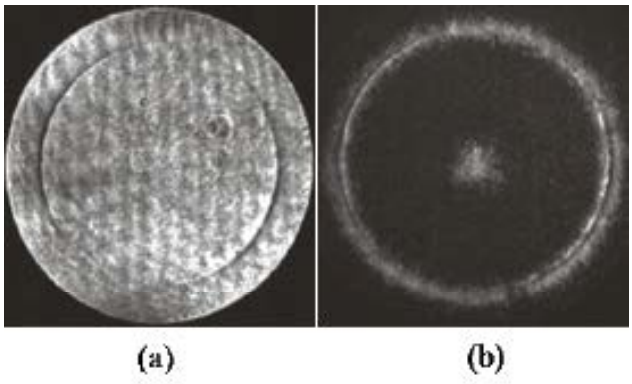

Figure 2 (a) Unmodulated back focal plane images of 50 nm gold samples and (b) amplitude modulated back focal plane image.

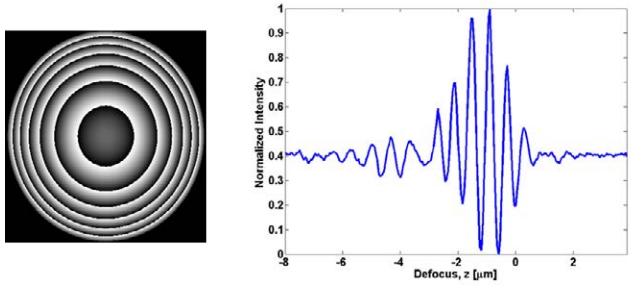

Figure 3 (a) defocus phase pattern (b) V(z) measurement of a single point in the image plane.

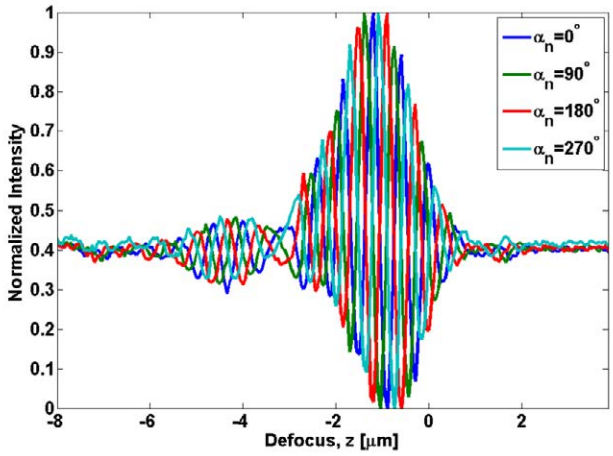

Figure 4 V(z) curves with 90 degrees phase step.

confocal phase SPR system is shown in **Figure 5**. The light source used in the system is 10 mW He-Ne laser at 633 nm free space wavelength. The laser beam magnified at the magnification stage is projected on the amplitude-modulating SLM's surface (LETO Holoeye SLM), where it undergoes amplitude modulation controlled by computer-generated modified Hadamard sequences. The amplitude modulated optical beams are then projected on the phase SLM's surface (PLUTO–NIR-011 Holoeye SLM) where corresponding phase profile (defocus and pupil mask) is introduced. After passing through another magnification stage, which matches the size of the phase-SLM screen and the size of the objective lens back focal plane (BFP), both amplitude and phase modulated illumination patterns are projected onto the sample by 1.25 NA objective lens (1.25 NA oil immersion objective by Zeiss). The same objective lens captures the light reflected by the sample. Two CCD cameras, the same magnifying optics and two beam splitters are used to capture the images of the image and back focal planes. The confocal pinhole is formed by a digitally at the image plane by processing the images obtained by the CCD camera. This allows us to change the size of the pinhole in the post processing stage.

Amplitude modulation is implemented using an SLM, which modulates intensity profile of the incident light by switching individual pixels ON and OFF, as it is illustrated by **Figure 6**. Independently controllable SLM's pixels open the way to create illumination patterns, which bear no correlation with one another. This allows us to maintain confocal effect for every individual amplitude SLM pixel, since every illumination/ detection point is interference-free from the rest. A Hadamard code provides a convenient illumination sequence, since it will generate efficient orthogonal sequence. This is used to produce amplitude modulated signal in this project.

Original Hadamard code, H_O, is a linear block code of $N=2^n$ length, comprising 1's and -1's and every line of code is correlated with itself only. However, it is not possible to implement negative intensity and therefore -1's are going to be replaced with 0's in illumination (modified Hadamard code H_M). In 1D intensity distribution $I(x)$ at the image plane of the microscope, using amplitude-modulated illumination, is a 2D matrix:

$$I(x,N)=\sum_i H_{Mi}(N)\left[S(x)\otimes O(x)\right], \quad (3)$$

Where $S(\chi)$ is the sample function and $O(\chi)$ is the intensity point-spread function of the microscope, subscript "i" denotes individual lines of modified Hadamard code, and $\otimes$ is a convolution operator.

In order to recover individual confocal images of the sample $I_{conf}(x)$, generated due to the different illumination patterns, $I(x,N)$ needs to be correlated with original Hadamard illumination patterns, but since modified Hadamard code must have a zero mean to maintain orthogonality the mean value must be subtracted from $I(x,N)$ first:

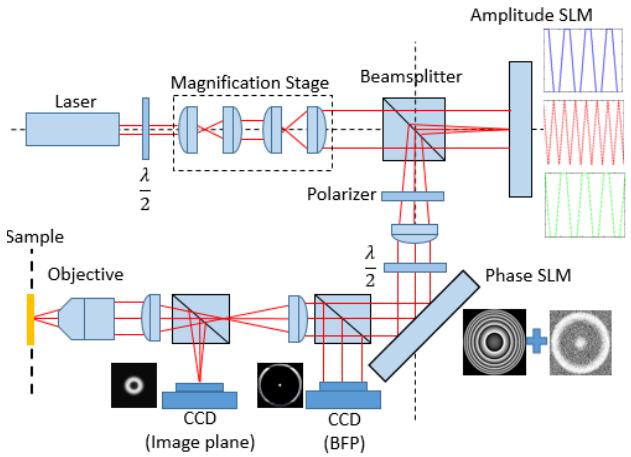

Figure 5 The microscope system diagram of the proposed widefield confocal surface plasmon microscope.

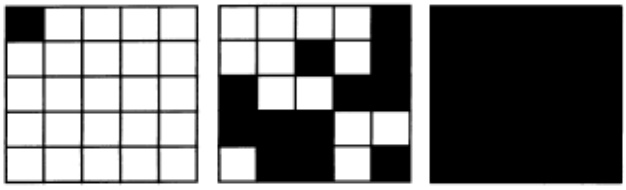

Figure 6 SLM screens with ON (white) and OFF (black) pixels.

$$I^{k}_{conf}(x) = \left[I(x,N) - \mu(I(x,N))\right] \bullet H_{Ok}, \quad (4)$$

$$I^{k}_{conf}(x) = \sum_{i} \left\{ \frac{H_{Mi}(N)}{2} \left[S(x) \otimes O(x)\right] \right\} \bullet H_{Ok} = (N/2)\left[S(x) \otimes O(x)\right], \quad (5)$$

where "*k*" is the index of the pattern used to test the image against and $k=i$ is a dot-product operator. Only when $k = i$, the value of $I^{k}_{conf}(x)$ will be nonzero, thus preserving confocality of individual images in multipoint scanning arrangement. The process of confocal image recovery is illustrated in **Figure 7**.

Since, both amplitude and phase modulation are required in order to achieve multipoint *V(z)* scan, the total number of 2D images captured by the image CCD camera is a product of Hadamard sequence length and number of defocus scan points. For every given defocus value, the whole Hadamard sequence must be obtained.

Results

In order to extract the SPR related information, every Hadamard-coded stack of images, for the given defocus value, must be processed, according to the Equation (4). Then, confocal pinholes must be defined and placed on the recovered individual point-spread functions, and finally, the plasmon resonance angle can be extracted for every confocal pixel using the Equation (2) or from the gradient of *φ(z)*.

Figure 8 shows the *V(z)* curve results recovered from 128-bit long Hadamard sequence and (b) recovered *φ(z)*. It can be seen form the figure that the Hadamard sequence allows us to have a better quality signal and signal to noise ratio is much better than the results shown in **Figure 3b**. This is for a single point measurement.

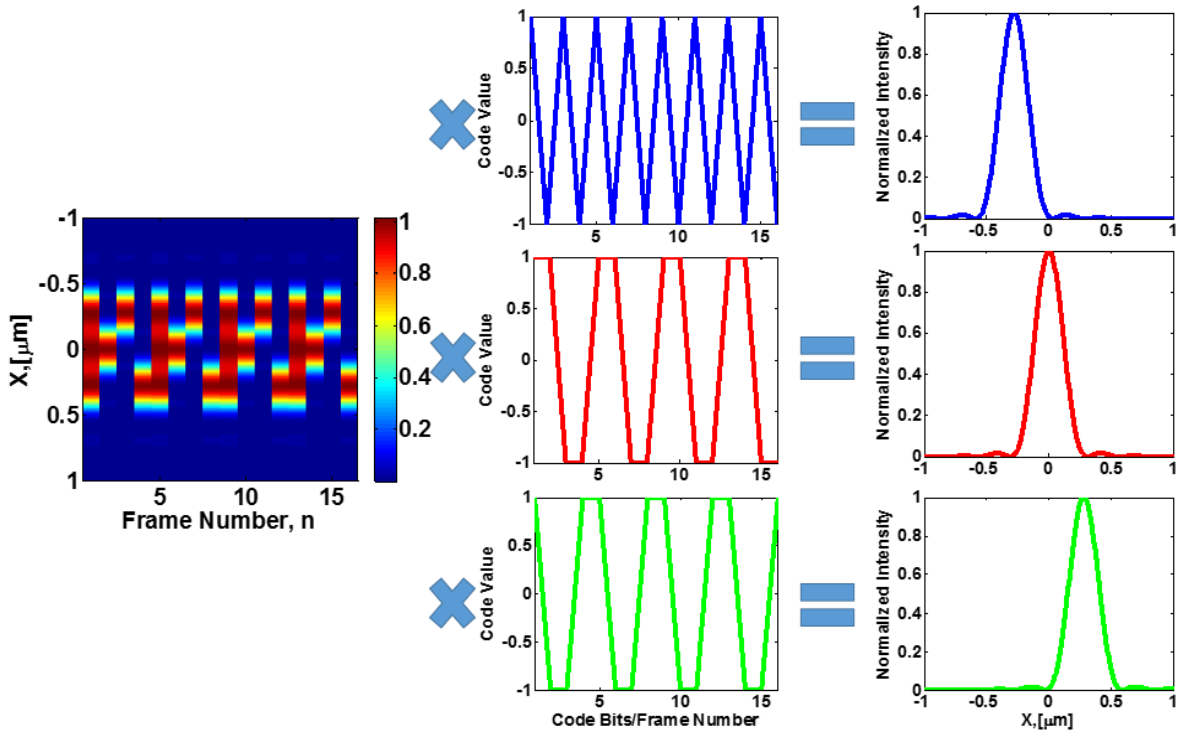

Figure 7 Confocal image recovery (a) I(x, N), (b) HO and (c) Ikconf (x).

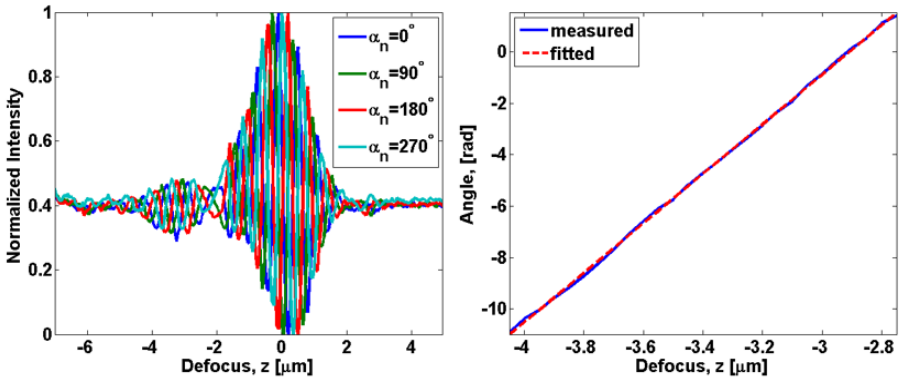

Figure 8 **(a)** *V(z)* curves for 128-bit long Hadamard sequence and **(b)** recovered *φ(z)*.

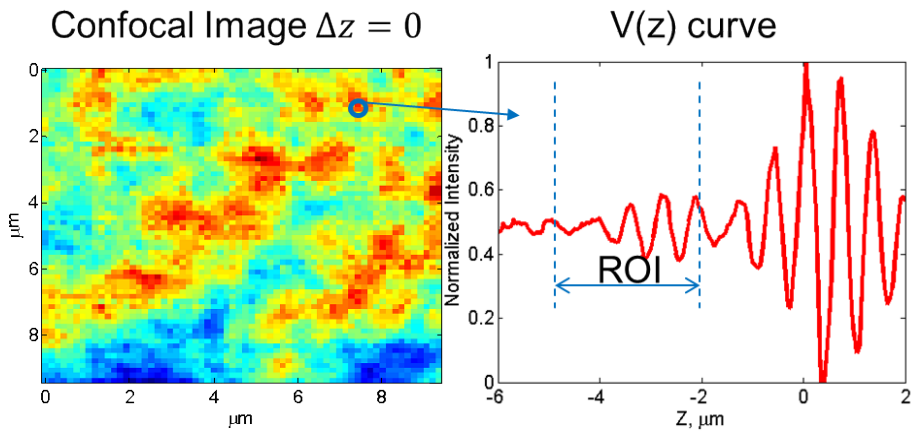

Figure 9 **(a)** V*(x, y)* at z=0 µm and **(b)** *V(z)* curve corresponding to the marked position in (a).

The next step, we took multiple points measurement as shown in **Figure 9**. It can be seen from the figure that the method allows us to take a confocal image for each z defocus slice.

Discussion

Confocal imaging is very broadly employed not only in the field of material science but also in cell physiology [29], histology [30], and neuroscience [31]. Especially in the fast-growing field of living tissue/organ imaging. We believe that the high speed parallel focal spots imaging is very crucial in such biological imaging. In the previous section, we have demonstrated how the widefield confocal surface plasmon microscope works and how the system speeds up the confocal imaging. In this section, we will discuss some issues of the current system.

Signal to noise ratio and input light intensity

The current system was designed and aligned to ensure that the image plane was illuminated with a uniform beam profile. This was achieved by magnifying the Gaussian HeNe laser beam profile by 35 times. Less than 3% of the 10mW power arrives the CCD camera because of the magnification and necessary optical beam splitters. This has forced us to use quite a long Hadamard sequence, i.e., 128 bits to recover a decent signal.

Temperature stability

We found that the experimental results obtained during the night time were more reliable than the experimental results obtained during the day time. This might be because of the bigger temperature fluctuation during the day time. We will enclose the system, control the temperature and humidity in the laboratory. If necessary, we will use an objective PID temperature control kit to ensure that the objective lens temperature is stable.

Spatial light modulator speed

The SLMs that we are using in the system is very slow. The crystal response time is around 0.1s. It therefore takes very long acquisition time. This makes the temperature fluctuation and drifting effect more severe.

Non-zero background amplitude SLM and low scattering light level

The amplitude SLM that we use in the system cannot produce a true zero intensity background level and the light scatter from a pixel is very low. This makes the point spread functions appear as a very faint signal on top of a non-zero background. This degrades the signal to noise ration and forces us to use a longer Hadamard sequence to recover the signal.

Conclusion

In this paper, we have explained and demonstrated how our proposed widefield confocal surface plasmon microscope measure the complex k-vector of surface plasmons. The system requires two spatial light modulators. Firstly, a phase-SLM aligned in a conjugate plane of objective back focal plane provides electronic defocus and amplitude pupil function modulation in the back focal plane. Secondly, an amplitude SLM aligned in a conjugate plane of objective lens image plane provides Hadamard sequential coding in the image plane. The coded images are then stored and the confocal image can be recovered by the method described in details in the Materials and Methods section. However, there are a number of issues that need to be addressed, such as, the non-zero background intensity of the amplitude SLM, the signal to noise and the speed of the SLMs. These issues will be addressed and reported in a later publication.

References

1 Schasfoort RB (2017) Handbook of surface plasmon resonance. Royal Society of Chemistry, UK.

2 Pechprasarn S, Somekh MG (2014) Detection limits of confocal surface plasmon microscopy. Biomed Opt Express 5(6): 1744-1756.

3 Pongruengkiat W, Pechprasarn S (2017) Whispering-gallery mode resonators for detecting cancer. Sensors 17(9): 2095.

4 Suvarnaphaet P, Pechprasarn S (2018) Enhancement of long-range surface plasmon excitation, dynamic range and figure of merit using a dielectric resonant cavity. Sensors 18(9): 2757.

5 Tan HM, Pechprasarn S, Zhang J, Pitter MC, Somekh MG (2016) High resolution quantitative angle-scanning widefield surface plasmon microscopy. Sci Rep 6: 20195.

6 Somekh MG, Pechprasarn S (2016) Surface plasmon, surface wave, and enhanced evanescent wave microscopy. Handbook of Photonics for Biomedical Engineering 1-41.

7 Pechprasarn S, Learkthanakhachon S, Zheng G, Shen H, Lei DY, et al. (2016) Grating-coupled Otto configuration for hybridized surface phonon polariton excitation for local refractive index sensitivity enhancement. Opt Express 24(17): 19517-30.

8 Pechprasarn S, Chow TW, Somekh MG (2018) Application of confocal surface wave microscope to self-calibrated attenuation coefficient measurement by Goos-Hänchen phase shift modulation. Sci Rep 8(1): 8547.

9 Abayzeed SA, Smith RJ, Webb KF, Somekh MG, See CW (2017) Sensitive detection of voltage transients using differential intensity surface plasmon resonance system. Opt Express 25(25): 31552-67.

10 Huang Y, Xia L, Wei W, Chuang CJ, Du C (2014) Theoretical investigation of voltage sensitivity enhancement for surface plasmon resonance based optical fiber sensor with a bimetallic layer. Opt Commun 333: 146-50.

11 Fang N, Xi D, Xu J, Ambati M, Srituravanich W, et al. (2006) Ultrasonic meta-materials with negative modulus. Nat Mater 5(6): 452.

12 Lin TJ, Chung MF (2009) Detection of cadmium by a fiber-optic biosensor based on localized surface plasmon resonance. Biosens Bioelectron 24(5): 1213-8.

13 Wang LV (2009) Multiscale photoacoustic microscopy and computed tomography. Nat Photonics 3(9): 503.

14 Vasconcelos TL, Archanjo BS, Fragneaud B, Oliveira BS, Riikonen J, et al. (2015) Tuning localized surface plasmon resonance in scanning near-field optical microscopy probes. ACS Nano 9(6): 6297-304.

15 Berguiga L, Zhang S, Argoul F, Elezgaray J (2007) High-resolution surface-plasmon imaging in air and in water: V (z) curve and operating conditions. Opt Lett 32(5): 509-11.

16 Wei H, Wang Z, Tian X, Käll M, Xu H (2011) Cascaded logic gates in nanophotonic plasmon networks. Nat Commun 2: 387.

17 Edwards B, Engheta N (2012) Experimental verification of displacement-current conduits in metamaterials-inspired optical circuitry. Phys Rev Lett 108(19): 193902.

18 Shadrivov IV, Zharov AA, Kivshar YS (2003) Giant Goos-Hänchen effect at the reflection from left-handed metamaterials. Appl Phys Lett 83(13): 2713-5.

19 Huidobro PA, Fernández-Domínguez AI, Pendry JB, Martín-Moreno L, Garcia-Vidal FJ (2018) Spoof Surface Plasmon Metamaterials. Cambridge University Press. USA.

20 Sheng P, Stepleman RS, Sanda PN (1982) Exact eigenfunctions for square-wave gratings: Application to diffraction and surface-plasmon calculations. Phys Rev B 26(6): 2907.

21 Ferry VE, Sweatlock LA, Pacifici D, Atwater HA (2008) Plasmonic nanostructure design for efficient light coupling into solar cells. Nano Lett 8(12): 4391-7.

22 Barnes WL, Dereux A, Ebbesen TW (2003) Surface plasmon sub-wavelength optics. Nature 424(6950): 824.

23 Kretschmann E, Raether H (1968) Radiative decay of non radiative surface plasmons excited by light. Z Naturforsch A 23(12): 2135-2136.

24 Pechprasarn S, Somekh M (2012) Surface plasmon microscopy: resolution, sensitivity and crosstalk. J Microsc 246(3): 287-297.

25 Pechprasarn S, Zhang B, Albutt D, Zhang J, Somekh M (2014) Ultrastable embedded surface plasmon confocal interferometry. Light Sci Appl 3(7): e187.

26 Zhang B, Pechprasarn S, Somekh MG (2012) Surface plasmon microscopic sensing with beam profile modulation. Opt Express 20(27): 28039-28048.

27 Zhang B, Pechprasarn S, Somekh MG (2013) Quantitative plasmonic measurements using embedded phase stepping confocal interferometry. Opt Express 21(9): 11523-11535.

28 Zhang B, Pechprasarn S, Zhang J, Somekh MG (2012) Confocal surface plasmon microscopy with pupil function engineering. Opt Express 20(7): 7388-7397.

29 Yan J, Thomson JK, Zhao W, Gao X, Huang F, et al. (2018) Role of stress kinase JNK in Binge alcohol-evoked atrial arrhythmia. J Am Coll Cardiol 71(13): 1459-1470.

30 Yan J, Thomson JK, Wu X, Zhao W, Pollard AE, et al. (2014) Novel methods of automated quantification of gap junction distribution and interstitial collagen quantity from animal and human atrial tissue sections. PLoS One 9(8): e104357.

31 Iwasaki S, Ikegaya Y (2018) *In vivo* one-photon confocal calcium imaging of neuronal activity from the mouse neocortex. J Integr Neurosci 2: 1-8.